Potential Energy Surfaces for Ligand Exchange Reactions of Square Planar Diamagnetic PtY_2L_2 Complexes: Hydrogen Bond ($PtY_2L_2\cdots L'$) *versus* Apical ($Y_2L_2Pt\cdots L'$) Interaction

Jong Keun Park* **and Bong Gon Kim**

*Department of Chemistry Education and Research Institute of Natural Science, Gyeongsang National University, Jinju 660-701, Korea. *E-mail: mc7@gsnu.ac.kr*

Received April 19, 2006

The geometrical structures, potential energy surfaces, and energetics for the ligand exchange reactions of tetracoordinated platinum (PtY_2L_2 : Y, L=Cl^-, OH^-, OH_2, NH_3) complexes in the ligand-solvent interaction systems were investigated using the *ab initio* Hartree-Fock (HF) and Density Functional Theory (DFT) methods. The potential energy surfaces for the ligand exchange reactions used for the conversions of ($PtCl_4$ + H_2O) to [$PtCl_3(H_2O)$ + Cl^-] and [$Pt(NH_3)_2Cl_2$ + H_2O] to [$Pt(NH_3)_2Cl(H_2O)$ + Cl^-] were investigated in detail. For these two exchange reactions, the transition states ($[PtY_2L_2\cdots L']^{\ddagger}$) correspond to complexes such as ($PtCl_4\cdots H_2O)^{\ddagger}$ and $[Pt(NH_3)_2Cl_2\cdots H_2O]^{\ddagger}$, respectively. In the transition state, ($[PtCl_4\cdots H_2O]^{\ddagger}$ and $[Pt(NH_3)_2Cl_2\cdots H_2O]^{\ddagger}$) have a kind of 6-membered (Pt-Cl$\cdots$HOH$\cdots$Cl) and (Pt-OH$\cdots$Cl$\cdots$HN) interactions, respectively, wherein a central Pt(II) metal directly combines with a leaving Cl^- and an entering H_2O. Simultaneously, the entering H_2O interacts with a leaving Cl^-. No vertical one metal-ligand interactions ($[PtY_2L_2\cdots L']^{\ddagger}$) are found at the axial positions of the square planar (PtY_2L_2) complexes, which were formed *via* a vertically associative mechanism leading to D_{3h} or C_{2v}-transition state symmetry. The geometrical structure variations, molecular orbital variations (HOMO and LUMO), and relative stabilities for the ligand exchange processes are also examined quantitatively. Schematic diagrams for the dissociation reactions of {$PtCl_4(H_2O)_n(n = 2,4)$} into {$PtCl_3(H_2O)_{(n-2)}$ + $Cl^-(H_2O)_2$} and the binding energies {$PtCl_4(H_2O)_n(n = 1\text{-}5)$} of $PtCl_4$ with water molecules are drawn.

Key Words : Geometrical structures, Potential energy surfaces, Ligand exchange reactions, Atomic charge, Density functional theory

Introduction

Recently, the anti-tumor properties of square planar platinum (PtY_2L_2) complexes have been studied with various theoretical and experimental techniques.[1-29] The properties of these complexes were investigated by focusing on the ligand exchange reactions *via* the interaction between the metal and ligands/solvents. The ligand exchange reactions of these Pt(II) complexes are suggested to proceed *via* a five-coordinated transition state with an axial metal-ligand interaction.[1-12] These ligand exchange processes are also characterized by electron density transfers from the neutrally and negatively charged ligands to the central Pt(II) metal and the leaving L groups. The charge values of the central metal are dependent on the contribution of the charges transferred from the electron pair of the ligands. Since the unoccupied $d_{x^2-y^2}$ orbital interacts with the lone pair orbitals of the ligands, the structural characteristic of Pt(II) stereochemistry is the tendency to form square planar Pt(II) complexes.

In terms of the reaction mechanisms associated with the ligand exchanges at the planar d^8 center, some studies[1-7] reported that the reaction proceeds *via* a five-coordinated transition state ($[PdL_5]^{\ddagger}$) with a D_{3h} (C_{2v})-trigonal bipyramidal structure, while others studies[8,9] reported that it proceeds *via* a C_1-transition state structure. In the studies conducted by the Deeth group,[1,2] the ligand exchange reactions were suggested to occur *via* a vertically associative mechanism leading to C_{2v}-transition state symmetry ($[PdL_5]^{\ddagger}$). The transition state structure of $[PdL_5]^{\ddagger}$ is very similar to the C_{2v}-trigonal bipyramidal symmetry both energetically and geometrically. But the structure of transition state does not conform to rigorous trigonal bipyramidal geometry (D_{3h}). The bond lengths of the equatorial (M-OH_2) bonds are 0.25 - 0.30 Å longer than those of the axial bonds. The energetic diagrams for the hydration processes of platinum complexes were examined by Burda *et al.*[3-5] All the transition states of the Pt complexes form five-coordinated trigonal bipyramids. The five stationary steps in the S_N2 pathway for the *cis*platin hydrolysis are characterized by Zhang *et al.*[6] and Costa *et al.*[7] In the transition states, the structures of the complexes are also optimized to the five-coordinate trigonal bipyramids.

In the studies by Chval and Sip,[8] the geometrical structures of the *cis*platin for the S_N2 hydrolysis reactions were optimized. At the transition state for the hydrolysis reaction, the transition states have a distorted trigonal bipyramid with

* The Corresponding Author is an executive research worker of educational research institute in GSNU.

considerably prolonged bonds to the leaving and entering ligands. Meanwhile, in the aqueous solution system, the geometrical structures of the axially coordinated tetraaqua and tetrachloro Pt(II) complexes ($[PtCl_4]^{2-}\cdot(H_2O)_2$, $[Pt(H_2O)_4]^{2+}\cdot(H_2O)_8$) were optimized by the Muñoz-Páez group.[9] Although the two axially oriented water ligands in $[PtCl_4]^{2-}\cdot(H_2O)_2$ were optimized, one oxygen atom in the water molecule does not bond to the planar d^8 center of the Pt(II) complex. The two hydrogen atoms of the water ligand situated above and below the planar center on the vertical axis interact with the two chloride atoms, respectively. Using the radial distribution functions, the solvation shells surrounding the $[PtCl_4]^{2-}$ complexes were investigated by the Naidoo group.[10] There is no evidence of an axial water molecule approaching through the δ^- oxygen atom to the δ^+ metal atom of either complex. Experimentally, two vertical metal-oxygen interactions at the apical positions of the square planar $PtCl_4^{2-}$ complexes were observed by Caminiti *et al.*[15] The interactions between the metal atom and the two water molecules situated apically occur from a larger distance with respect to the chlorine ligands. The geometrical structure of $[MCl_4]^{2-}\cdot(H_2O)_2$ by the metal-oxygen interaction is a distorted octahedral complex. With the replacement of one or more Cl^- ions with water molecules, the possible solvation mechanisms of the ligand exchange in the square-planar complexes implies a ligand-solvent interaction and/or metal-solvent interaction.

Although the reaction mechanisms for the ligand exchange of the Pt(II) complexes have already been studied by some groups, the potential energy surfaces through the ligand exchange processes has not yet been investigated. Further investigations would seem to be worthwhile on the basis of the following points. (i) The ligand exchange reactions of tetracoordinated *cis*platin (PtY_2L_2) complexes were reported to proceed through a five-coordinated transition state (C_{2v} or C_1-symmetry). In this respect, do the reactions proceed through five- or six-coordinated transition states or intermediates with C_{2v} or C_1-symmetry? (ii) In the ligand-solvent interaction system, ($PtY_2L_2\cdots L'$) complexes with a hydrogen bond between the ligand and solvent or pentacoordinated ($Y_2L_2Pt\cdots L'$) complexes with an apical (Pt $\cdots$L') interaction may exist. These complexes are different from each other. Which type interactions are really ligand-solvent complexes? (iii) How many transition states and intermediates can exist on the potential energy surfaces of the conversion from the reactants (PtY_2L_2 + L') to the product (PtY_2LL' + L)? (iv) Is the barrier height of the potential energy surfaces high or low? (v) Is the reaction involving the formation of (PtY_2LL' + L) from (PtY_2L_2 + L') endothermic or exothermic? To answer these questions, we studied the potential energy surfaces and the energy contour maps for the ligand exchange reactions of tetracoordinated PtY_2L_2 complexes. Our detailed potential energy surfaces and energy contour maps for the tetracoordinated Pt(II) complexes are greatly dependent on the characteristics of the ligands complexed with the Pt(II) metal.

Computational Methods

The equilibrium geometrical structures of (PtY_2L_2 : Y, L = Cl^-, OH^-, OH_2, NH_3) in the ground state (singlet state) were fully optimized with the Hartree-Fock (HF), second-order Möller-Plesset (MP2), and density functional theory (DFT) levels using the Gaussian 03.[30,31] The hybrid DFT (B1LYP, B3LYP, B3P86) density functional utilizes the exchange functional of Becke[32] in conjunction with Lee-Yang-Parr correlation functional[33] and gives good structural and energetic informations even for relatively large chemical systems such as transition metal complexes. To confirm the existence of stable structures, the harmonic vibrational frequencies of the species were analyzed at the DFT level. In addition, the atomic charges of the natural bond orbital (NBO) of the equilibrium (PtY_2L_2) complexes were also analyzed in order to investigate the charge transfer of the ligand exchanges. The effective core potential including the relativistic contributions is used to represent the 46 innermost electrons of the Pt atom (lanl2dz). The standard 6-31G* basis sets are used for the other atoms (H, N, O, Cl).

The potential energy surfaces of the ligand exchange reactions from (PtY_2L_2 + L') to (PtY_2LL' + L) are calculated for $R_{Pt\text{-}L}$ and $R_{Pt\text{-}Y}$ using the B1LYP method. The potential energy curves from ($PtCl_4$ + H_2O) to ($PtCl_3(OH_2)$ + Cl^-) are calculated using the total energies as a function of the (Pt-O) distances in the range of 2.3 to 4.53 Å and the (Pt-Cl) distances in the range of 2.3 to 6.0 Å. The potential curves from [$Pt(NH_3)_2Cl_2$ + H_2O] to [$Pt(NH_3)_2Cl(OH_2)$ + Cl^-] are calculated using the total energies as a function of the (Pt-O) distances in the range of 2.2 to 4.25 Å and the (Pt-Cl) distances in the range of 2.2 to 4.25 Å. The schematic diagrams for the dissociation reactions of $\{PtCl_4(H_2O)_n(n = 2,4)\}$ into $\{PtCl_3(H_2O)_{(n-2)} + Cl^-(H_2O)_2\}$ are calculated using the total energies as a function of the (Pt-Cl) distances in the range of the reactants to the product asymptotes. And the binding energies $\{PtCl_4(H_2O)_n(n = 1\text{-}5)\}$ of $PtCl_4$ with water molecules are also calculated stepwise.

Results and Discussion

The optimized internuclear (Pt-L) distances of the equilibrium geometrical structures of *cis*- and *trans*-PtY_2L_2 are listed in Table 1. The optimized distances at the DFT level are in good agreement with the previous theoretical[1-14,16-21] and experimental[15,22-29] values. The geometrical structures optimized at the HF, B1LYP, B3LYP, and B3P86 levels are the unsymmetrically square planar structures for PtY_2L_2 and the symmetrically square planar structures for PtL_4. The internuclear (Pt-L) distances of each complex at the HF level are longer than those of the corresponding complexes at the DFT levels. At the DFT levels, the internuclear (Pt-Cl), (Pt-N), and (Pt-O) distances of *trans*-PtY_2L_2 are similar to those of *cis*-PtY_2L_2, respectively. In the case of the PtL_4-type, the optimized $R_{Pt\text{-}O}$ distance of $[Pt(OH)_4]^{2-}$ is shorter than the others, while, the $R_{Pt\text{-}Cl}$ distance of $[PtCl_4]^{2-}$ is longer than

Table 1. Optimized (Pt-L) distances (Å) of the equilibrium geometrical structures of PtY_2L_2

	$PtCl_4^{2-}$	*trans*-$PtCl_2(OH)_2^{2-}$		*cis*-$PtCl_2(OH)_2^{2-}$		$Pt(OH)_4^{2-}$	*trans*-$PtCl_2(OH_2)_2$		*cis*-$PtCl_2(OH_2)_2$	
	R_{Pt-Cl}	R_{Pt-Cl}	R_{Pt-O}	R_{Pt-Cl}	R_{Pt-O}	R_{Pt-O}	R_{Pt-Cl}	R_{Pt-O}	R_{Pt-Cl}	R_{Pt-O}
HF	2.372	2.351	2.072	2.403	2.060	2.069	2.405	2.087	2.346	2.264
MP2	2.366	2.344	2.052	2.390	2.020	2.036	2.397	2.092	2.347	2.281
B1LYP	2.358	2.337	2.022	2.379	2.006	2.046	2.317	2.026	2.271	2.220
B3LYP	2.356	2.336	2.028	2.380	2.003	2.049	2.321	2.023	2.278	2.223
B3P86	2.352	2.334	2.027	2.377	2.004	2.045	2.320	2.024	2.276	2.222
HF[a]	2.33									
MP2[d]	2.329	2.338	2.026	2.372, 2.406	1.997, 1.980		2.289	2.024	2.238	2.109
MP2[e]							2.304, 2.286	2.003, 2.043	2.246, 2.253	2.076, 2.102
MP2[f]	2.364							2.360[b]		
ADF[h]	2.37, 2.30							2.400[b], 2.358[b]		
LDA[i]	2.35						2.32[j]	2.03[j]		
DFT[k]	2.422[l], 2.455[l]						2.352	2.072	2.299	2.158
DFT[m]	2.367									
exptl	2.310[n]									
	2.309[o]									
	2.315[p]									
	2.34[q], 2.32[q]									
	2.305[r], 2.32[r]									
	2.316[s]									
	2.308[t]									

Table 1. Continued

	$Pt(OH_2)_4^{2+}$	*trans*-$Pt(NH_3)_2(OH)_2^{2+}$		*cis*-$Pt(NH_3)_2(OH)_2^{2+}$		*trans*-$PtCl_2(NH_3)_2$		*cis*-$PtCl_2(NH_3)_2$		$Pt(NH_3)_4^{2+}$
	R_{Pt-O}	R_{Pt-O}	R_{Pt-N}	R_{Pt-O}	R_{Pt-N}	R_{Pt-Cl}	R_{Pt-N}	R_{Pt-Cl}	R_{Pt-N}	R_{Pt-N}
HF	2.082	2.072	2.074	2.085	2.087	2.296	2.059	2.277	2.063	2.069
MP2	2.082	2.061	2.067	2.083	2.084	2.293	2.052	2.272	2.060	2.062
B1LYP	2.078	2.053	2.056	2.072	2.073	2.287	2.041	2.257	2.054	2.054
B3LYP	2.076	2.052	2.057	2.073	2.075	2.288	2.044	2.259	2.053	2.058
B3P86	2.073	2.054	2.055	2.071	2.072	2.286	2.042	2.256	2.053	2.057
HF[c]								2.39	2.13	
HF[e]								2.343, 2.345	2.116, 2.132	
MP2[d]		2.033	2.049			2.293	2.025	2.275	2.056	2.055
MP2[e]						2.312, 2.284	2.023, 2.034	2.277	2.051	
MP2[b]						2.291	2.045	2.406[g]	2.123[g]	
MP2[b]				2.08	2.00			2.34	2.09	
MP4[c]								2.320, 2.312	2.105, 2.034	
mPW1PW[g]								2.368, 2.386	2.084, 2.085	
B3LYP[g]								2.411	2.110	
B3P86[b]				2.07	2.00			2.33	2.09	
LDA[i]	2.04[j], 2.01[j]			2.07	2.01	2.33	2.035	2.315	2.07, 2.065	
DFT[l]								2.368, 2.452	2.084, 2.155	
DFT[b]	2.049[f]					2.073	2.335	2.33	2.10	
DFT[b]						2.037	2.308	2.30[j]	2.05[j]	
exptl[u]						2.32 ± 0.01	2.05 ± 0.04	2.33 ± 0.01	2.01 ± 0.04	2.05[v]
exptl[u]								2.333, 2.328	1.950, 2.050	

[a]Ref. 17. [b]Ref. 8. [c]Ref. 21. [d]Ref. 3. [e]Ref. 5. [f]Ref. 9. [g]Ref. 11. [h]Ref. 18. [i]Ref. 20. [j]Ref. 1. [k]Ref. 12. [l]Ref. 6. [m]Ref. 13. [n]Ref. 26. [o]Ref. 27. [p]Ref. 15. [q]Ref. 22. [r]Ref. 28. [s]Ref. 25. [t]Ref. 29. [u]Ref. 23. [v]Ref. 24.

the others. The $R_{Pt\text{-}O}$ distance of $[Pt(OH_2)_4]^{2+}$ is similar to the $R_{Pt\text{-}N}$ distance of $[Pt(NH_3)_4]^{2+}$. In the PtY_2L_2-type, the optimized $R_{Pt\text{-}Cl}$ distance of *cis*-$[Pt(OH)_2Cl_2]^{2-}$ is longer than the others, while the optimized $R_{Pt\text{-}O}$ distance of *cis*-$[Pt(OH)_2Cl_2]^{2-}$ is shorter than the others. The optimized $R_{Pt\text{-}Cl}$, $R_{Pt\text{-}O}$, and $R_{Pt\text{-}N}$ distances of the PtY_2L_2 conformations are similar to the $R_{Pt\text{-}Cl}$ distance of $[PtCl_4]^{2-}$, the $R_{Pt\text{-}O}$ distance of $[Pt(OH)_4]^{2-}$, and the $R_{Pt\text{-}N}$ distance of $[Pt(NH_3)_4]^{2+}$, respectively. The symmetrical configuration and charge balance of the ligand around the central Pt(II) atom influence the bond length between Pt(II) and the ligands. In particular, the electronic neutralization between the positively charged Pt(II) metal and the negatively charged ligands contributes to the binding strength and stability of the square planar complexes.

To get a local minimum geometry having the five or six-coordinated Pt(II) complexes, although the fifth or sixth ligand is forced to approach the positively charged Pt(II) core at axially both sides, the fifth or sixth ligand moves automatically to the position marked by the long distance from the central Pt(II) core to make a tetracoordinated square planar complex. (a single occupied d_{z2}-orbital of the central Pt(II) metal interacts with each lone pair orbital of the ligands at the axially both sides, and the four ligands simultaneously interact with a $d_{x^2-y^2}$ orbital of the Pt(II) core metal) Therefore, the five or six-coordinated Pt(II) complexes in the platinum complexes cannot be optimized. In the transition state and product complexes, the five or six-coordinated Pt(II) complexes are not also optimized.

In the square planar PtY_2L_2 structures optimized by Deeth and Elding,[1,2] $R_{Pt\text{-}Cl}$ = 2.32 Å for *trans*-$Pt(H_2O)_2Cl_2$ and $R_{Pt\text{-}O}$ = 2.09 Å for *trans*-$Pt(H_2O)_2Cl_2$ were obtained. The optimized distances of the Pt complexes at the LDA level cause the (Pt-L) bond length to be increased by about 0.07 Å for $[Pt(H_2O)_4]^{2+}$. In the results of the Burda group,[3-5] the $R_{Pd\text{-}Cl}$ distance varies from 2.23 Å in the positively charged [*trans*-$Pt(NH_3)_2Cl(H_2O)]^+$ complex to 2.35 Å in the negatively charged [*cis*-$Pt(NH_3)Cl_2(OH)]^-$ complex. The longest (Pt-Cl) bond length is 2.406 Å in *cis*-$[Pt(OH)_2Cl_2]^{2-}$, while the shortest (Pt-O) bond length is 1.94 Å in [*cis*-$Pt(NH_3)_2(H_2O)(OH)_2]^+$. In the negatively charged complexes, the (Pt-L) distances are longer than those in the neutral complexes. According to the results of Chval and Sip,[8] the horizontally $R_{Pt\text{-}Cl}$ and $R_{Pt\text{-}N}$ distances of *cis*platin are 2.30 Å and 2.05 Å, respectively. And the vertically (Pt(II)···O) distance is 2.967 Å. As a result, the central Pt(II) atom of the *cis*platin can hardly be considered penta-coordinated complex. According to the results of Wysokinski and Michalska,[11] the mPW1PW hybrid model provides the best prediction of the (Pt-N) and (Pt-Cl) bond lengths in *cis*platin. In the geometrical structures of *cis*platin optimized by Pavankumar *et al.*,[21] these bond distances ($R_{Pt\text{-}Cl}$, $R_{Pt\text{-}N}$) are sensitive to the level of electron correlation and the size of the basis sets. In the case of the higher correlation level and larger basis sets, the bond distances are very close to the experimental values. All optimized (Pt-L) distances of PtY_2L_2 exceed the corresponding experimental values. The interaction between Pt^{2+} and L^- is of a kind of ionic coordinative character, so that the interaction between the two ions becomes stronger and the distance between two ions becomes shorter. Meanwhile, in the structures of axially coordinated $\{[Pt(H_2O)_4]^{2+}\cdot(H_2O)_8\}$ and $\{[PtCl_4]^{2-}\cdot(H_2O)_2\}$ complexes optimized by the Muñoz-Páez group,[9] The optimized (Pt-Cl) distance in the equatorial $[PtCl_4]^{2-}$ units is 2.352 Å, while the optimized (Pt-O) distance in the axial Pt-water is 3.288 Å. The length of the (Pt-Cl) bond is about 1 Å shorter than that of the (Pt-O) bond. In the $[Pt(H_2O)_4]^{2+}\cdot(H_2O)_8$ complex, the eight oxygen atoms of the eight water ligands in the second solvation shell only form hydrogen-bonds to the eight hydrogen atoms of the four water molecules situated in the inner solvation shell.

In the previously experimental results,[15,22-29] the shortest and longest (Pt-Cl) distances of the crystal $[PtCl_4]^{2-}$ structures are 2.305 and 2.34 Å, respectively. The average experimental $R_{Pt\text{-}Cl}$ value of $[PtCl_4]^{2-}$ is 2.316 Å. In the study of Caminiti *et al.*,[15] the $R_{Pt\text{-}Cl}$ distance in the first coordination shell (square-planar $[MCl_4]^{2-}$ units) is 2.315 Å, while the M-O distance of the metal-H_2O interactions bonded to the apical position is 2.77 Å. The interactions between the metal and the two water molecules situated apically occur from the larger distance with respect to the equatorially chloride ligands. It was suggested that the interaction between the complex and the solvent in aqueous solutions originates from the solubility of the $[PtCl_4]^{2-}$ complexes. In the study of Bengtsson and Oskarsson,[28] the internuclear $R_{Pt\text{-}Cl}$ distances are influenced by the solid/solution states and the measuring techniques/methods. An $R_{Pt\text{-}Cl}$ distance of 2.305 Å was reported for the crystal like $(NH_4)_2PtCl_4$ based on the X-ray diffraction pattern, while an $R_{Pt\text{-}Cl}$ distance of 2.32 Å was obtained for an aqueous solution of H_2PtCl_4 by means of the LAXS technique. In the study of Milburn and Truter,[23] the $R_{Pt\text{-}Cl}$ (2.32 ± 0.01 Å) and $R_{Pt\text{-}N}$ (2.05 ± 0.04 Å) distances of *trans*platin are similar to the $R_{Pt\text{-}Cl}$ (2.33 ± 0.01 Å) and $R_{Pt\text{-}N}$ (2.01 ± 0.04 Å) distances of *cis*platin, respectively. Although the geometries of these Pt complexes were optimized at the higher computational level, all of the optimized (Pt-L) distances are slightly longer than those obtained in the experimental analysis in the solid/solution states.[15,22-29] The differences between the calculated and experimental distances are attributable to the effects of the solid/solution environments, such as hydrogen bonding and crystal packing.

The potential energy surface and contour map for the ligand exchange processes of ($\{([PtCl_4]^{2-}\cdots OH_2)$, **A**$\}$ → $\{([PtCl_3]^-\cdots[OH_2][Cl^-])$, **B**$\}$ → $\{([PtCl_3(OH_2)]^-\cdots Cl^-)$, **C**$\}$) are presented in Figures 1 and 2, respectively. The internuclear distances are from 2.3 to 4.53 Å for (Pt-O) and from 2.3 to 6.0 Å for (Pt-Cl). To make the energy surface more understandable, we indicated **A**, **B**, and **C** in Figures 1 and 2. **A** and **C** are stable positions for both the reactant and product, and **B** is a transition state. **A** and **C** are not the positions of the asymptotes. At the **A** position, $([PtCl_4]^{2-}\cdots OH_2$, with two hydrogen bond interactions ($R_{(Cl\cdots H_2O)}$ = 2.253 Å) is optimized. That is, the two of the chlorine

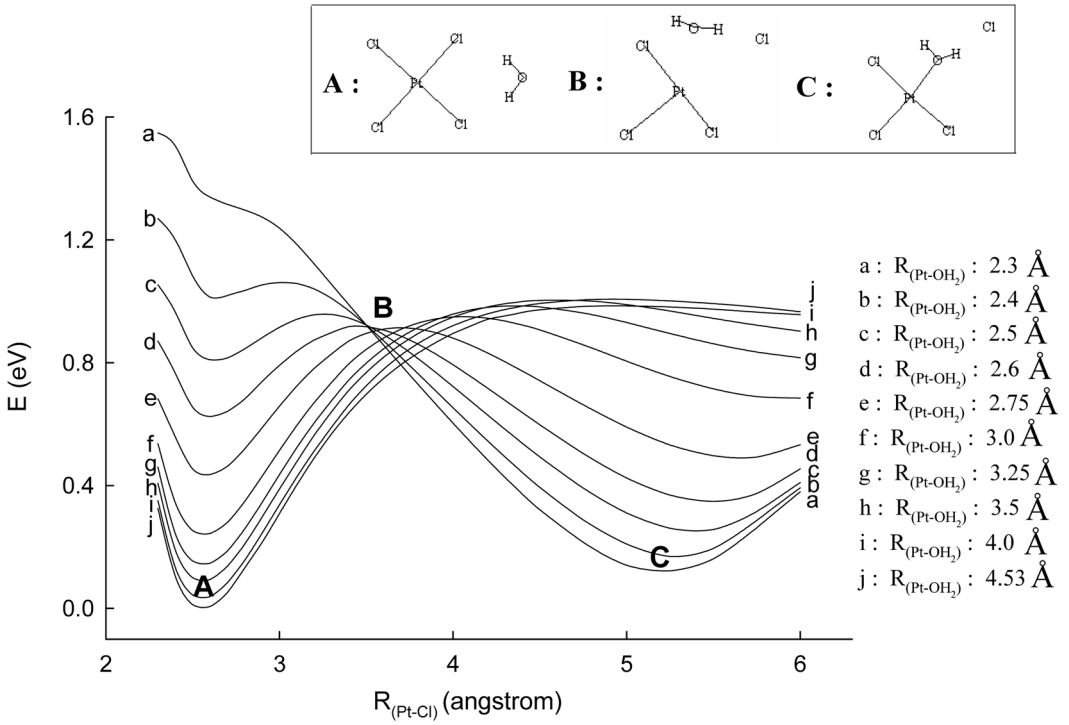

Figure 1. Potential energy surface for the ligand exchange processes involving the reactant {($[PtCl_4]^{2-}\cdots OH_2$), **A**}, the transition state {($[PtCl_3]^{-}\cdots[OH_2][Cl^{-}]$), **B**}, and the product {($[PtCl_3(OH_2)]^{-}\cdots Cl^{-}$), **C**}. All energies are adiabatic values and are in units of eV.

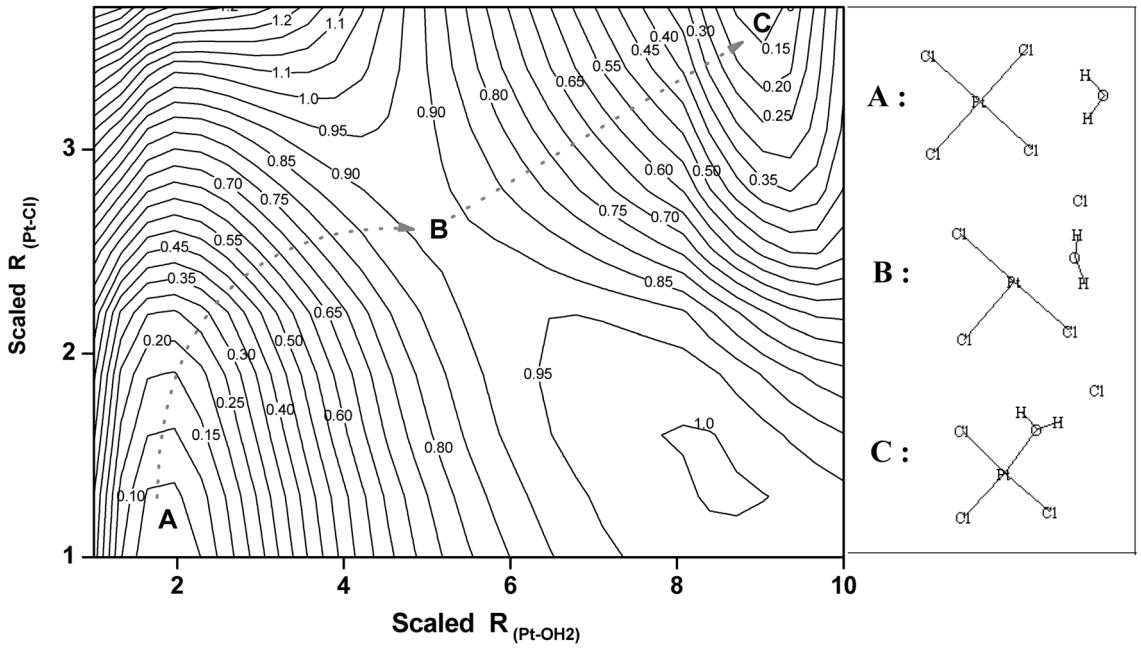

Figure 2. Energy contour map of the ligand exchange processes involving the reactant {($[PtCl_4]^{2-}\cdots OH_2$), **A**}, the transition state {($[PtCl_3]^{-}\cdots[OH_2][Cl^{-}]$, **B**), and the product {($[PtCl_3(OH_2)]^{-}\cdots Cl^{-}$), **C**}.

ligands of $[PtCl_4]^{2-}$ directly interact with the two hydrogen atoms of H_2O. The geometrical structure of ($[PtCl_4]^{2-}\cdots OH_2$) is a completely planar type. No vertical one or two metal-ligand interactions ($[Cl_4Pt\cdots OH_2]$, $[Cl_4Pt\cdots(OH_2)_2]$) were found at the axial position of the square planar ($PtCl_4$) complexes. To obtain a local minimum geometry having the vertical metal-ligand $[Cl_4Pt\cdots OH_2]$ complex in the equilibrium state, although the oxygen atom of the water molecule is forced to approach the positively charged Pt(II) core at the vertical position, the water molecule automatically moves toward the chlorine atom of $[PtCl_4]^{2-}$ to make a hydrogen bond. Therefore, the $[Cl_4Pt\cdots OH_2]$ complex cannot be optimized with a vertical metal-ligand interaction at the axial position.

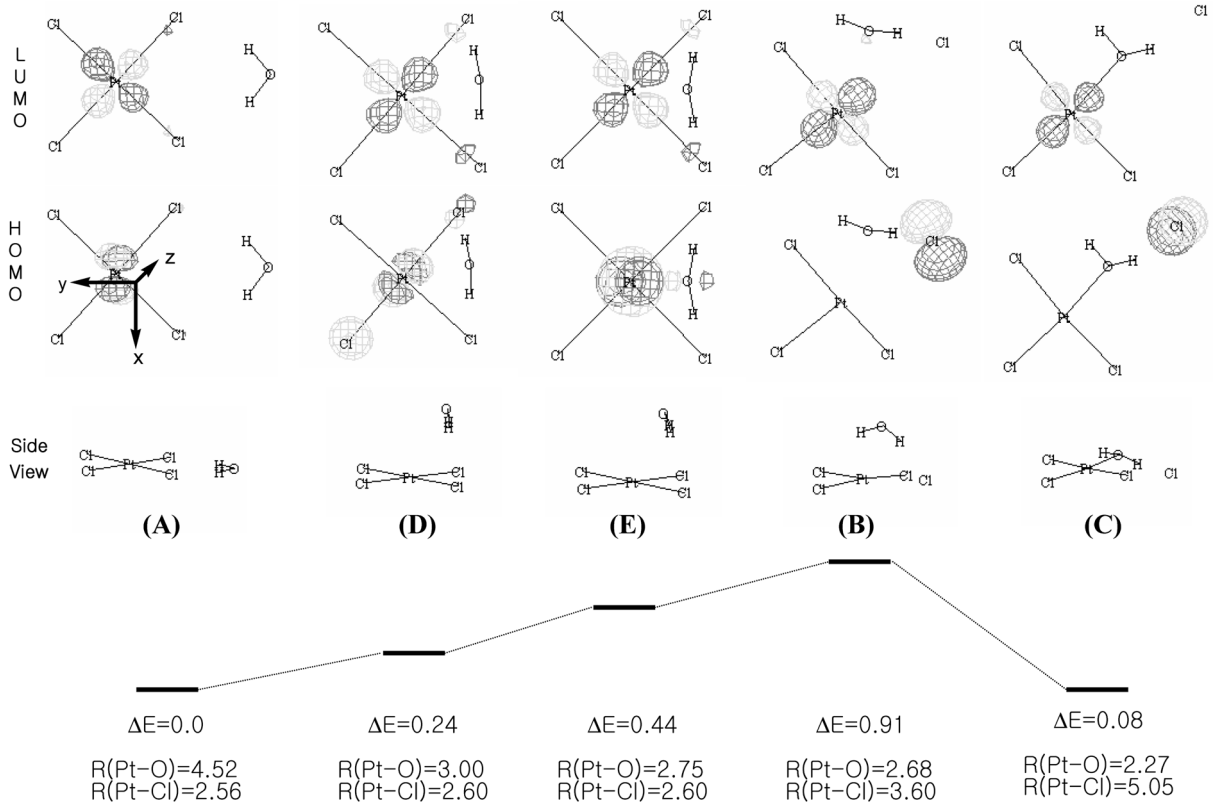

Figure 3. Geometrical structures, relative potential energies, and HOMO/LUMO for the ligand exchange process involving the reactant {($[PtCl_4]^{2-}\cdots OH_2$), **A**}, the transition state {($[PtCl_3]^-\cdots[OH_2][Cl^-]$), **B**}, and the product {($[PtCl_3(OH_2)]^-\cdots Cl^-$), **C**}. All energies are adiabatic values and are in units of eV. Bond lengths are in angstroms.

The potential energy surface has a transition state at **B**. By replacing one ligand with another, an optimized structure for the transition state in the ligand exchange processes is obtained which is a distorted Pt complex with a 6-membered (Pt-Cl$\cdots$HOH$\cdots$Cl) interaction. A central Pt(II) metal in the transition state combines with an entering H_2O and a leaving Cl^-. Simultaneously, the entering H_2O forms a hydrogen-bond with a leaving Cl^-. The $R_{Pt\text{-}O}$ and $R_{Pt\text{-}Cl}$ distances at **B** are 2.684 and 3.595 Å, respectively. At point **C**, the stable structure with the hydrogen bond ($R_{(Cl\cdots H_2O)}$=2.029 Å) between H_2O and Cl^- is optimized. No vertical one metal-ligand interactions [$Cl_3(H_2O)Pt\cdots Cl$] were found at the apical position of $[PtCl_3(OH_2)]^-$, which were formed *via* a D_{3h} or C_{2v}-transition state symmetry. To obtain a local minimum geometry at **C**, although Cl^- is forced to approach the Pt(II) metal at the vertical position, Cl^- also moves toward the hydrogen atom of the water molecule to make a hydrogen bond. Figure 2 shows only the potential energy surfaces produced by the projection for the 3-demensional axis (x-$R_{(Pt\text{-}Cl)}$, y-$R_{(Pt\text{-}O)}$, z-energy axis) of Figure 1. From the reactant of ($[PtCl_4]^{2-}\cdots OH_2$) to the product of ($[PtCl_3(OH_2)]^-\cdots Cl^-$), the ligand exchange reactions take place through the transition state surface. The broken lines indicate the estimated potential valley surfaces and these are drawn by hand. This transition complex is formed with a 6-membered interaction including Pt, Cl^-, and OH_2. The binding energies of this **B** state relative to the reactant and product are 0.91 and 0.82 eV, respectively. The ligand exchange reactions from ($[PtCl_4]^{2-}\cdots OH_2$) to ($[PtCl_3(OH_2)]^-\cdots Cl^-$) are very slightly endothermic and nearly isoenergetic.

To clarify the mechanism of the ligand exchange reactions, the variations of the geometrical structures, relative potential energies, and HOMO/LUMO were investigated in detail using five sets of reaction coordinates (from **A** for $R_{Pt\text{-}O}$ = 4.52 Å and $R_{Pt\text{-}Cl}$ = 2.56 Å to **C** for $R_{Pt\text{-}O}$ = 2.27 Å and $R_{Pt\text{-}Cl}$ = 5.05 Å) and the results are represented in Figure 3. The potential energy of the {($[PtCl_4]^{2-}\cdots OH_2$), **A**} complex is set to zero. The HOMO and LUMO are represented as the top view. At the **A** position, ($[PtCl_4]^{2-}\cdots OH_2$) has a planar structure with C_{2v}-symmetry. The d_{xz}-orbital of the central Pt atom is the HOMO and the $d_{x^2-y^2}$ orbital is the LUMO. At the **D** position, two of the chlorine atoms of $[PtCl_4]^{2-}$ continuously interact with the two hydrogen atoms of H_2O. The water molecule is located on the upside of the square planar $[PtCl_4]^{2-}$ complex. The angles of $\angle$ Pt-Cl-O and $\angle$ O-Pt-Cl are 60.1 and 71.1 degrees, respectively. The **D** position in Figure 3 corresponds to one point on the potential energy curve, **f**, in Figure 1. **D** in curve, **f**, is the lowest and most stable position. The relative energy of **D** with respect to **A** is 0.24 eV. The d_{xz}- and $d_{x^2-y^2}$-orbitals of the central Pt atom are the HOMO and LUMO, respectively. The HOMO of the d_{xz}-orbital is represented as the top view. The size of the HOMO of the *trans* Cl and leaving Cl atoms is increased by changing the reaction coordinates.

At the **E** position (R_{Pt-O} = 2.75 Å and R_{Pt-Cl} = 2.60 Å), two of the chlorine atoms of $[PtCl_4]^{2-}$ still interact with the two hydrogen atoms of H_2O. The water molecule is axially located on the square planar $[PtCl_4]^{2-}$ complex. The angles of ∠ Pt-Cl-O and ∠ O-Pt-Cl are 54.9 and 74.3 degrees, respectively. The metal-ligand interactions correspond to neither ∠ O-Pt-Cl = 90.0° nor C_{2v}-symmetry. In Figure 1, **E** in the **e** curve is the lowest and most stable position. The relative energy of **E** with respect to **A** is 0.44 eV. The d_{z^2}- and $d_{x^2-y^2}$-orbitals of the central Pt atom are also the HOMO and LUMO, respectively. The interaction of the d_{z^2}-orbital with one of the oxygen atoms at the HOMO is strengthened. As the distance between the central Pt atom and water ligand decreases, the d_{z^2}-HOMO combines with the p-orbital of the oxygen atom in the water molecule.

At the **B** position (R_{Pt-O} = 2.684 Å and R_{Pt-Cl} = 3.595 Å), the chlorine atom of a (Pt-Cl) bond is disconnecting from $[PtCl_4]^{2-}$ and Pt(II) is simultaneously interacting with an H_2O molecule. The water molecule is located on the upside of the $[PtCl_4]^{2-}$ complex. The angles of ∠ Pt-Cl-O, ∠ O-Pt-Cl, and ∠ Cl-O-Pt are 46.8, 55.4, and 77.7 degrees, respectively. The metal-ligand interaction corresponds to neither ∠ O-Pt-Cl = 90.0° nor C_{2v}-symmetry. No vertical metal-ligand interactions ($[PtY_2L_3]^{\ddagger}$) were found at the apical position of the square planar ($PtCl_4$) complexes. The potential energy surface has one transition state corresponding to complexes such as $(PtCl_4 \cdots H_2O)^{\ddagger}$. In Figure 1, **B** is the highest and most unstable position in the potential energy surfaces. The relative energy of **B** with respect to **A** is 0.91 eV. The d_{xz}-orbital is the HOMO and the $d_{x^2-y^2}$ orbital is the LUMO. The size of the HOMO of the leaving Cl^- is increased by changing the reaction coordinates. As the distance between Pt(II) and the water molecule decreases, the d_{z^2}-HOMO combines with the p-orbital of the oxygen atom in the water molecule. At the **C** position (R_{Pt-O} = 2.27 Å and R_{Pt-Cl} = 5.05 Å), a new (Pt-O) bond is formed. One of the hydrogen atoms of the H_2O molecule still forms a hydrogen-bond with the leaving Cl^- group. The geometry of the product corresponds to a nearly planar structure. The relative energy of **C** with respect to **A** is 0.08 eV. The *p*-orbital of the leaving Cl^- is the HOMO and the $d_{x^2-y^2}$ orbital is the LUMO.

The potential energy surface and contour map for the ligand exchange processes of ({$([Pt(NH_3)_2Cl_2] \cdots H_2O$), **A**} → {$([Pt(NH_3)_2Cl]^+ \cdots [H_2O][Cl^-]$), **B**} → {$([Pt(NH_3)_2Cl(H_2O)]^+ \cdots Cl^-$), **C**}) are presented in Figures 4 and 5, respectively. The internuclear distances are from 2.2 to 4.25 for (Pt-O) and from 2.2 to 4.25 for (Pt-Cl). To make the energy surface easy to understand, we have just represented **A**, **B**, and **C** in Figures 4 and 5. **A** and **C** correspond to the equilibrium positions of the reactant and product, respectively, and **B** is the point corresponding to the transition state. At position **A**, $([Pt(NH_3)_2Cl_2] \cdots H_2O)$ with two horizontal ligand-solvent interactions ($R_{(Cl \cdots H_2O)}$=2.228 Å, $R_{(H_2NH \cdots OH_2)}$=2.228 Å) is optimized. That is, the two chlorine atoms of $[Pt(NH_3)_2Cl_2]$ interact horizontally with the two hydrogen atoms of H_2O. By hydrogen bonding, a 6-membered interaction is formed

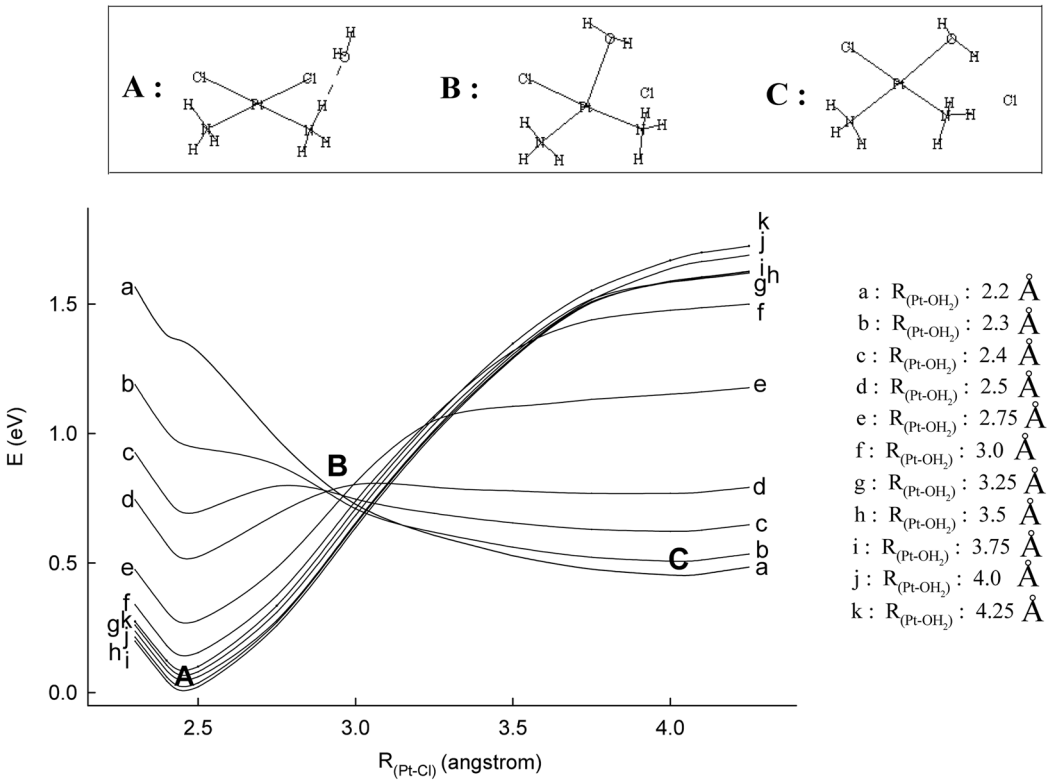

Figure 4. Potential energy surface for the ligand exchange processes of *cis*platin involving the reactant {$([Pt(NH_3)_2Cl_2] \cdots H_2O$), **A**}, the transition state {$([Pt(NH_3)_2Cl]^+ \cdots [H_2O][Cl^-]$), **B**}, and the product {$([Pt(NH_3)_2Cl(H_2O)]^+ \cdots Cl^-$), **C**}. All energies are adiabatic values and are in units of eV.

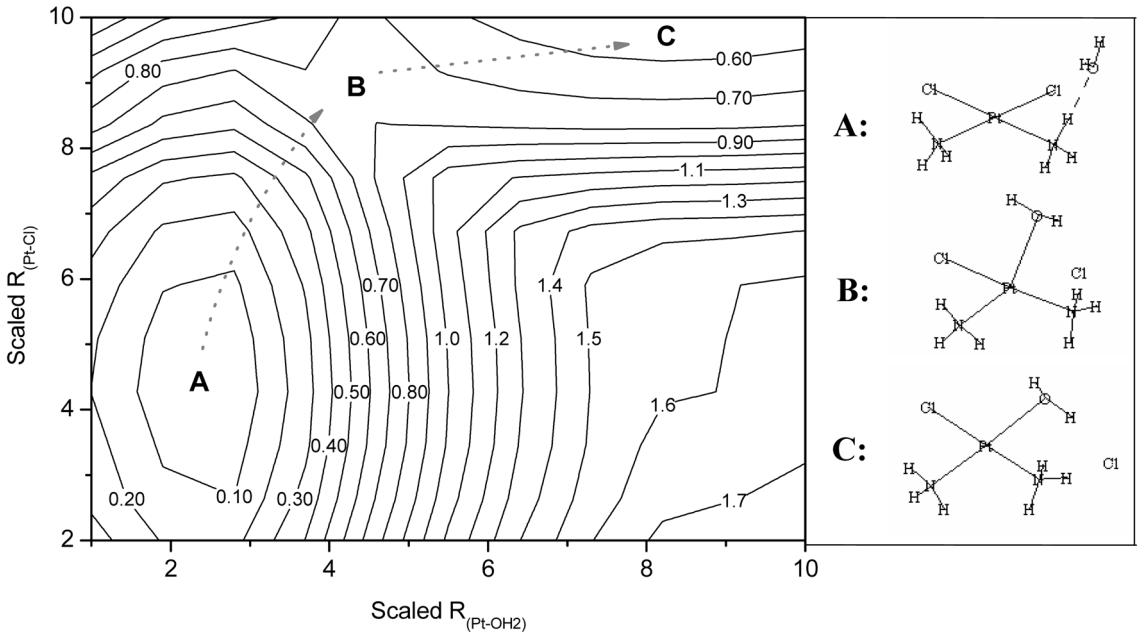

Figure 5. Energy contour map of the ligand exchange processes involving the reactant {($[Pt(NH_3)_2Cl_2]\cdots H_2O$), **A**}, the transition state {($[Pt(NH_3)_2Cl]^+\cdots[H_2O][Cl^-]$), **B**}, and the product {($[Pt(NH_3)_2Cl(H_2O)]^+\cdots Cl^-$), **C**}.

from the *cis*platin and water. The interaction is located on the planar Pt complex. No vertical one or two metal-ligand interactions ($[(NH_3)_2Cl_2Pt\cdots OH_2]$, $[(NH_3)_2Cl_2Pt\cdots(OH_2)_2]$) were found at the axial position of the square planar ($Pt(NH_3)_2Cl_2$) complex. To obtain a vertical metal-ligand ($[(NH_3)_2Cl_2Pt\cdots OH_2]$) complex in the equilibrium state, although an oxygen atom of the water ligand is forced to approach the positively charged Pt(II) core at the vertical position, the ligand automatically optimizes its position in relation to the chlorine atom of the square planar $[Pt(NH_3)_2Cl_2]$ complex to make a hydrogen bond. As a result, the $[(NH_3)_2Cl_2Pt\cdots OH_2]$ complex with the vertical metal-ligand interaction at the axial position cannot be optimized. The potential curve of **i** ($R_{Pt\text{-}O}$ = 3.75 Å) has the lowest energy level around the **A** position.

The potential energy surface has a transition state at **B**. At the transition state, the optimized structure for the ligand exchange processes is a pentacoordinated Pt complex with a 6-membered (Pt-OH$\cdots$Cl$\cdots$HN) interaction. The 6-membered interaction of this transition state is formed with Pt, Cl^-, and H_2O. The Pt(II) metal combines with an entering H_2O and a leaving Cl, and the entering H_2O simultaneously forms a hydrogen-bond with a leaving Cl^-. The distances $R_{Pt\text{-}O}$ and $R_{Pt\text{-}Cl}$ at **B** are 2.486 and 2.942 Å, respectively. At point **C**, the stable structure with the hydrogen bond ($R_{(Cl\cdots H_2O)}$ = 1.882 Å, $R_{Cl\cdots HNH_2)}$ = 2.057 Å) between H_2O and Cl^- is optimized. No vertical one metal-ligand interactions were found ($[(NH_3)_2Cl_2Pt\cdots OH_2]$) at the apical position on the square planar $[Pt(NH_3)_2Cl_2]$ complex. To obtain a local minimum geometry, although a leaving Cl^- is forced to approach the positively charged Pt(II) metal at the vertical position, Cl^- moves to the hydrogen atom of the water molecule to form a hydrogen bond. Figure 5 shows the projection of Figure 4 for the 3-demensional axis (x-$R_{(Pt\text{-}Cl)}$, y-$R_{(Pt\text{-}O)}$, z-energy axis). From the reactant ($[Pt(NH_3)_2Cl_2]\cdots OH_2$) to the product ($[Pt(NH_3)_2Cl(OH_2)]^+\cdots Cl^-$), the ligand exchange reactions take place through the transition state surface. The direction of the reaction path for the ligand exchange processes is denoted by the broken lines on the contour map. The broken lines indicate the estimated potential valley surfaces and these are drawn by hand. The ligand exchange reactions from ($[Pt(NH_3)_2Cl_2]\cdots OH_2$) to ($[Pt(NH_3)_2Cl(OH_2)]^+\cdots Cl^-$) are slightly endothermic.

The variations in the geometrical structures, relative potential energies, and HOMO/LUMO were investigated using five sets of reaction coordinates (from **A** for $R_{Pt\text{-}O}$ = 3.61 Å and $R_{Pt\text{-}Cl}$ = 2.475 Å to **C** for $R_{Pt\text{-}O}$ = 2.20 Å and $R_{Pt\text{-}Cl}$ = 3.90 Å) and the results are represented in Figure 6. The potential energy of the {($[Pt(NH_3)_2Cl_2]\cdots H_2O$), **A**} complex is set to zero. The HOMO and LUMO are represented as the top view. At the **A** position, one of the chlorine atoms of $[Pt(NH_3)_2Cl_2]$ interacts with one of the hydrogen atoms of H_2O. Simultaneously, one of the hydrogen atoms of NH_3 interacts with the oxygen atom of H_2O. In *cis*-$[Pt(NH_3)_2Cl_2]\cdots H_2O$, a 6-membered interaction is formed by means of two hydrogen bonds. The geometry of (*cis*-$[Pt(NH_3)_2Cl_2]\cdots H_2O$) is not a planar structure. The d_{xz}-orbital of the central Pt metal is the HOMO and the $d_{x^2\text{-}y^2}$ orbital is the LUMO. At the **D** position ($R_{Pt\text{-}O}$ = 2.75 Å and $R_{Pt\text{-}Cl}$ = 2.47 Å), the two hydrogen-bonds (between Cl of $[Pt(NH_3)_2Cl_2]$ and H of H_2O, between H of NH_3 and O of H_2O) are still to be found. The water molecule is axially located on the square planar $[Pt(NH_3)_2Cl_2]$ complex. The angles of Pt-N-O and O-Pt-N are 65.7 and 65.4 degrees, respectively. The angles of Pt-Cl-O and O-Pt-Cl are 57.3 and 73.6 degrees, respectively. In Figure 6, the **D** position corresponds to a point on the

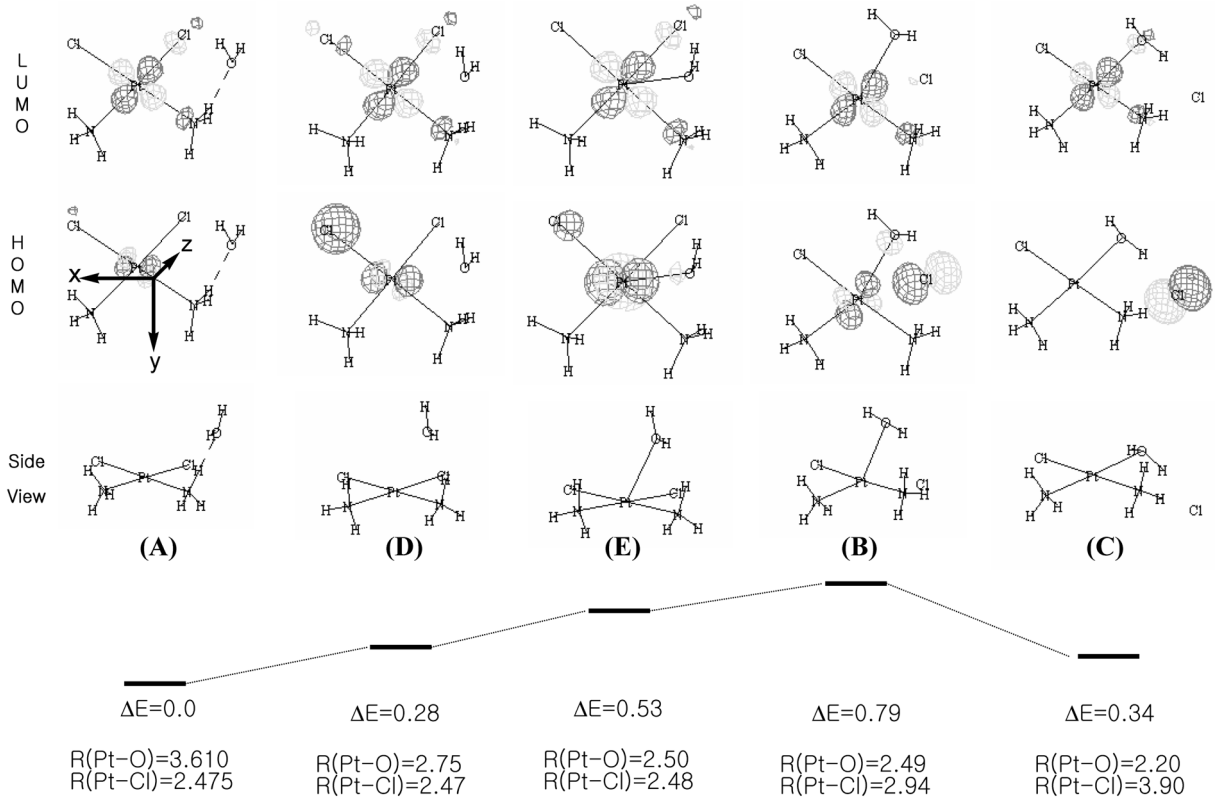

Figure 6. Schematic diagram for the ligand exchange processes involving the reactant {($[Pt(NH_3)_2Cl_2]\cdots H_2O$), A}, the transition state {($[Pt(NH_3)_2Cl]^+\cdots[H_2O][Cl^-]$), B}, and the product {($[Pt(NH_3)_2Cl(H_2O)]^+\cdots Cl^-$), C}, including the HOMO and LUMO of the complexes. All energies are adiabatic values and are in units of eV. Bond lengths are in angstroms.

potential energy curve, **e**, in Figure 4. **D** in curve **e** is the lowest and most stable position. The relative energy of **D** with respect to **A** is 0.28 eV. The d_{xz}-orbital of Pt is still the HOMO and the $d_{x^2-y^2}$ orbital is the LUMO. The size of the HOMO of the *cis*-Cl and leaving Cl atoms is increased. At the **E** position (R_{Pt-O} = 2.50 Å and R_{Pt-Cl} = 2.48 Å), one of the Cl atoms of $[Pt(NH_3)_2Cl_2]$ forms a hydrogen-bond with one of the H atoms of H_2O, and one of the H atoms of NH_3 simultaneously forms a hydrogen-bond with the O atom of H_2O. The water molecule is vertically located on the square planar $[Pt(NH_3)_2Cl_2]$ complex. The angles of ∠ Pt-N-O and ∠ O-Pt-N are 57.7 and 71.8 degrees, respectively. The angles of ∠ Pt-Cl-O and ∠ O-Pt-Cl are 52.1 and 76.6 degrees, respectively. In Figure 4, the point, R_{Pt-O} = 2.50 Å and R_{Pt-Cl} = 2.48 Å, on the potential energy curve, **d**, corresponds to **E,** and **E** is the lowest and most stable position. The relative energy of **E** with respect to **A** is 0.53 eV. The d_{z^2}-orbital in the complex is the HOMO and the $d_{x^2-y^2}$ orbital is the LUMO. As the distance between Pt and water decreases, the d_{z^2}-HOMO increasingly interacts with the p-orbital of the oxygen atom in the water molecule.

At the **B** position (R_{Pt-O} = 2.486 Å and R_{Pt-Cl} = 2.942 Å), the chlorine atom of the (Pt-Cl) bond is disconnecting from $[Pt(NH_3)_2Cl_2]$ and Pt(II) is simultaneously interacting with the oxygen atom in H_2O. The leaving Cl^- of $[Pt(NH_3)_2Cl_2]$ still forms a hydrogen-bond with one of the H atoms of H_2O. The water molecule is located on the upside of the square planar $[Pt(NH_3)_2Cl_2]$ complex and the (Pt-O) bond is shorter than that of **E**. The angles of ∠ Pt-N-O and ∠ O-Pt-N are 49.3 and 87.0 degrees, respectively. The angles of ∠ Pt-Cl-O, ∠ O-Pt-Cl, and ∠ Cl-O-Pt are 49.4, 67.2, and 64.4 degrees, respectively. At the transition state, the structure formed from the central Pt, the entering H_2O, and the leaving Cl^- also consists of a 6-membered interaction. No vertical one metal-ligand interactions ($[Pt(NH_3)_2Cl_2\cdots(H_2O)]^{\ddagger}$) were found at the axial position of the square planar ($Pt(NH_3)_2Cl_2$) complexes. The potential energy surface has one transition state corresponding to a ($[Pt(NH_3)_2Cl]^+\cdots[H_2O][Cl^-]$)‡ complex. In Figure 4, the point, **B** (R_{Pt-O} = 2.486 Å and R_{Pt-Cl} = 2.942 Å), which is the highest and most unstable position. The relative energy of **B** with respect to **A** is 0.79 eV. The *p*-orbital of the leaving Cl^- is the HOMO and the $d_{x^2-y^2}$ orbital is the LUMO. As the distance between the central Pt atom and water molecule decreases, the size of the d_{z^2}-HOMO of the central Pt atom decreases and the sizes of the HOMOs of the entering H_2O and leaving Cl^- groups increase. At the **C** position (R_{Pt-O} = 2.20 Å and R_{Pt-Cl} = 3.90 Å), the (Pt-Cl) bond is disconnected. The structure of $[Pt(NH_3)_2Cl(H_2O)]^+$ is rearranged so as to have a distorted square planar geometry. The leaving Cl^- group is horizontally located in the middle of the H_2O and NH_3 molecules and connected with two hydrogen-bonds. The leaving Cl^- group in the 6-membered interaction is placed on the same plane as the Pt complex. The relative energy of **C** with

Table 2. Dissociation energies (eV) for the dissociation reactions of the equilibrium platinum (PtY_2L_2) complexes leading to their conversion to their asymptotes ($PtY_2L + L$)

Complex	L	HF	MP2	B1LYP	B3LYP	B3p86	EHT[a]
$[PtCl_4]^{2-}$	$\Delta E(Cl^-)$	1.17	1.64	1.01	0.97	1.05	0.58
trans-$[Pt(OH)_2Cl_2]^{2-}$	$\Delta E(Cl^-)$	1.53	1.52	1.48	1.48	1.49	
	$\Delta E(OH^-)$	3.19	3.13	3.08	3.07	3.08	
cis-$[Pt(OH)_2Cl_2]^{2-}$	$\Delta E(Cl^-)$	1.48	1.48	1.44	1.45	1.44	
	$\Delta E(OH^-)$	3.34	3.32	3.27	3.25	3.26	
$[Pt(OH)_4]^{2-}$	$\Delta E(OH^-)$	2.89	2.83	2.70	2.70	2.80	
trans-$Pt(OH_2)_2Cl_2$	$\Delta E(Cl^-)$	1.73	1.75	1.69	1.68	1.67	
	$\Delta E(OH_2)$	3.23	3.23	3.12	3.13	3.10	
cis-$Pt(OH_2)_2Cl_2$	$\Delta E(Cl^-)$	1.88	1.84	1.79	1.78	1.78	
	$\Delta E(OH_2)$	2.12	2.12	2.07	2.07	2.06	
$[Pt(OH_2)_4]^{2+}$	$\Delta E(OH_2)$	2.55	2.53	2.49	2.49	2.51	
trans-$[Pt(NH_3)_2(OH_2)_2]^{2+}$	$\Delta E(NH_3)$	2.66	2.63	2.62	2.62	2.63	
	$\Delta E(OH_2)$	2.65	2.62	2.60	2.61	2.61	
cis-$[Pt(NH_3)_2(OH_2)_2]^{2+}$	$\Delta E(NH_3)$	2.59	2.59	2.57	2.56	2.57	
	$\Delta E(OH_2)$	2.58	2.57	2.55	2.55	2.56	
trans-$Pt(NH_3)_2Cl_2$	$\Delta E(Cl^-)$	1.75	1.74	1.72	1.72	1.71	
	$\Delta E(NH_3)$	2.79	2.74	2.73	2.72	2.73	
cis-$Pt(NH_3)_2Cl_2$	$\Delta E(Cl^-)$	1.80	1.77	1.76	2.75	1.76	
	$\Delta E(NH_3)$	2.69	2.68	2.66	2.66	2.65	
$[Pt(NH_3)_4]^{2+}$	$\Delta E(NH_3)$	2.64	2.60	2.51	2.52	2.52	

[a]Ref. 19.

respect to **A** is 0.34 eV. Our results for the formation of $([Pt(NH_3)_2Cl(H_2O)]^+ \cdots Cl^-)$ from $([Pt(NH_3)_2Cl_2] \cdots H_2O)$ are slightly endothermic and nearly isoenergetic. The *p*-orbital of the leaving Cl^- is the HOMO and the $d_{x^2-y^2}$ orbital is the LUMO. By the results of Costa *et al*.,[7] the relative energies for the hydrolysis and reverse reactions of *cis*platin are 1.06 and 0.83 eV, respectively. By the results of Zhang *et al*.,[6] the relative enthalpies for the hydrolysis and reverse reactions of *cis*platin are 0.97 and 0.85 eV, respectively.

The relative energies for the dissociation reactions of (PtY_2L_2) into ($PtY_2L + L$) are listed in Table 2. The dissociation energies of the PtL_4 types determined at the B1LYP level are in the range of 1.01 eV for $[PtCl_4]^{2-}$ to 2.70 eV for $[Pt(OH)_4]^{2-}$. The dissociation energy of (Pt-OH) is the largest. Because the extent of the charge transfer from the negatively charged OH^- ligand to the positively charged Pt(II) atom increases, the strength of the (Pt-OH) bond increases. That is, due to the character of the ionic bond emerging from the cation-anion pair of $[Pt^{2+} + 4L^-]$, the dissociation energies and relative energy gaps for the dissociation of $[PtL_4]^{2-}$ into $([PtL_3]^- + L^-)$ are found to be relatively large. In the PtY_2L_2 type, the dissociation energies of the (Pt-L) bond at the *trans* position are quite different from those at the *cis* position. In *cis*-$[Pt(OH)_2Cl_2]^{2-}$, the dissociation energy ($\Delta E_{(OH-)}$ = 3.27 eV) of the (Pt-OH) bond is the largest, while the energy ($\Delta E_{(Cl-)}$ = 1.44 eV) of the (Pt-Cl) bond is the smallest. In *trans*- and *cis*-$[Pt(NH_3)_2(OH_2)_2]^{2+}$, the dissociation energies of the ($Pt-NH_3$) bond are similar to those of the ($Pt-OH_2$) bond. Meanwhile, in $Pt(OH_2)_2Cl_2$ and $Pt(NH_3)_2Cl_2$, the dissociation energies of the (Pt-Cl) bond of both isomers are different from those of the ($Pt-OH_2$) and ($Pt-NH_3$) bonds. In *cis*platin (*cis*-$Pt(NH_3)_2Cl_2$), the dissociation energy of ($Pt-NH_3$) is larger than that of ($Pt-OH_2$) in *cis*-$Pt(OH_2)_2Cl_2$, while in *trans*platin (*trans*-$Pt(NH_3)_2Cl_2$), the energy of the ($Pt-NH_3$) bonds is smaller than that of the ($Pt-OH_2$) bonds in $Pt(OH_2)_2Cl_2$. The dissociation energy gaps for the (Pt-Cl) bonds of *cis*platin and *trans*platin are similar to each other. The geometrical structures of the transition metal complexes with chlorides and its molecular species were optimized by Ponec and Řeřicha.[19] The dissociation energy (0.58 eV) of the (Pt-Cl) bond in $[PtCl_4]^{2-}$ is only obtained from the energy difference between $[PtCl_4]^{2-}$ and its ($[PtCl_3]^- + Cl^-$) asymptotes. This dissociation energy is much smaller than the values that we obtained at the DTF level. The binding energies of the metal-olefin π-complexes of $[M(Cl_3)(C_2H_4)]^-$ were obtained by Noell and Hay.[16,17] The metal-olefin π-complexes are formed by the interaction between the anion of $[PtCl_3]^-$ and the π-orbital of C_2H_4. The binding energy of $[Pt(Cl_3)(C_2H_4)]^-$ is 1.24 eV.

The average atomic charges (au) in the natural bond orbital (NBO) analysis of PtY_2L_2 at the B1LYP level are listed in Table 3. Our calculated charge values are in good agreement with the previously calculated results.[8-14] For the equilibrium geometry, the charge value of Pt(II) is positive, whereas those of the four L ligands are negative. The atomic charge values of Pt(II) and L are relatively large. Depending on the L ligand, the atomic charges of Pt(II) and the four L ligands are different from each other. Our charge values for Pt(II) at the B1LYP level vary from 0.55 to 0.99 au and the values for the ligands vary from –0.44 to –1.11 au. In the *trans* and *cis* isomers, the charge of Pt(II) in the *trans* type is more positive than that in the *cis* type. In the PtL_4 type, the

Table 3. Average atomic charges (au) of the natural bond orbital (NBO) of PtY_2L_2 calculated by various methods and the atomic charges (au) of the two internuclear distances (R_{Pt-L} = 3.0, 4.0 Å) at the B1LYP level

		equilibrium							R_{Pt-L} = 3.0	R_{Pt-L} = 4.0
		HF	B1LYP	B3LYP	B3p86	MP[g]	MP2[h]	DFT[i]	DFT	DFT
$[PtCl_4]^{2-}$	Q_{Pt}[a]	0.651	0.550	0.551	0.552	0.48	0.37	0.537	0.548	0.545
	Q_{Cl}[b,e]	−0.606	−0.638	−0.630	−0.626	−0.62	−0.64	−0.631	−0.594	−0.550
	Q_{Cl}[f]								−0.721	−0.810
trans-$[Pt(OH)_2Cl_2]^{2-}$	Q_{Pt}[a]	0.660	0.714	0.708	0.706		0.47	0.758	0.608	0.548
	Q_{Cl}[b]	−0.633	−0.723	−0.717	−0.713		−0.75	−0.720	−0.700	−0.687
	Q_O[c,e]	−1.117	−1.044	−1.042	−1.043		−0.82	−1.119	−0.960	−0.920
	Q_O[f]								−1.077	−1.087
cis-$[Pt(OH)_2Cl_2]^{2-}$	Q_{Pt}[a]	0.790	0.662	0.658	0.656		0.48		0.620	0.609
	Q_{Cl}[b]	−0.800	−0.725	−0.718	−0.715		−0.72		−0.722	−0.686
	Q_O[c,e]	−1.153	−1.024	−1.014	−1.017		−0.85		−0.965	−0.933
	Q_O[f]								−1.016	−1.113
$[Pt(OH)_4]^{2-}$	Q_{Pt}[a]	0.867	0.721	0.719	0.715				0.704	0.653
	Q_O[c,e]	−1.123	−1.113	−1.103	−1.109				−1.054	−0.970
	Q_O[f]								−1.170	−1.231
trans-$Pt(OH_2)_2Cl_2$	Q_{Pt}[a]	0.845	0.784	0.775	0.761			0.751	0.762	0.723
	Q_{Cl}[b]	−0.697	−0.548	−0.529	−0.525			−0.565	−0.521	−0.514
	Q_O[c,e]	0.925	−0.935	−0.925	−0.923			−0.913	−0.930	−0.920
	Q_O[f]								−0.972	−0.977
cis-$Pt(OH_2)_2Cl_2$	Q_{Pt}[a]	0.785	0.695	0.688	0.691		0.51	0.57[L]	0.688	0.681
	Q_{Cl}[b]	−0.609	−0.440	−0.430	−0.426		−0.41	−0.46[L]	−0.406	−0.390
	Q_O[c,e]	−1.016	−0.955	−0.948	−0.948		−0.37	−0.98[L]	−0.953	−0.950
	Q_O[f]								−0.976	−0.978
$[Pt(OH_2)_4]^{2+}$	Q_{Pt}[a]	1.095	0.999	0.992	0.989				0.976	0.960
	Q_O[c,e]	−1.026	−0.950	−0.943	−0.945				−0.966	−0.945
	Q_O[f]								−1.006	−1.117
trans-$[Pt(NH_3)_2(OH_2)_2]^{2+}$	Q_{Pt}[a]	1.007	0.995	0.986	0.988		0.82	0.946	0.989	0.967
	Q_N[d,e]	−1.105	−1.017	−1.008	−0.975		−0.15	−1.070	−0.948	−0.940
	Q_N[f]								−1.005	−1.100
	Q_O[c,e]	−1.025	−0.972	−0.967	−0.982		−0.28	−0.971	−0.963	−0.957
	Q_O[f]								−1.011	−1.013
cis-$[Pt(NH_3)_2(OH_2)_2]^{2+}$	Q_{Pt}[a]	0.996	0.901	0.902	0.893		0.78		0.891	0.874
	Q_N[d,e]	−1.066	−0.982	−0.974	−0.973		−0.27		−0.942	−0.935
	Q_N[f]								−0.985	−1.047
	Q_O[c,e]	−1.001	−0.984	−0.980	−0.984		−0.39		−0.980	−0.975
	Q_O[f]								−0.978	−0.984
trans-$Pt(NH_3)_2Cl_2$	Q_{Pt}[a]	0.561	0.652	0.644	0.641		0.46	0.569	0.643	0.628
	Q_{Cl}[b]	−0.685	−0.577	−0.567	−0.565		−0.59	−1.042	−0.560	−0.546
	Q_N[d,e]	−1.083	−1.004	−1.002	−1.005		−0.09	−0.574	−0.988	−0.980
	Q_N[f]								−1.125	−1.149
cis-$Pt(NH_3)_2Cl_2$	Q_{Pt}[a]	0.562	0.632	0.627	0.616		0.44	0.46[L]	0.630	0.624
	Q_{Cl}[b]	−0.640	−0.502	−0.493	−0.492		−0.43	−0.49[L]	0.456	−0.427
	Q_N[d,e]	−1.120	−1.013	−1.012	−1.015		−0.23	−1.08[L]	−1.008	−0.981
	Q_N[f]								−1.133	−1.151
$[Pt(NH_3)_4]^{2+}$	Q_{Pt}[a]	0.817	0.767	0.760	0.758		0.65	0.749	0.752	0.740
	Q_N[d,e]	−1.103	−1.046	−1.041	−1.044		−0.18	−1.076	−1.012	−1.007
	Q_N[f]								−1.004	−1.040

[a]Atomic charges of Pt(II) in PtY_2L_2. [b]Atomic charges of Cl in PtY_2L_2. [c]Atomic charges of O in PtY_2L_2. [d]Atomic charges of N in *trans*-$Pt(NH_3)_2Cl_2$. [e]*trans*-L atom of PtY_2L_2 dissociating into $(PtY_2L\cdots L)$. [f]Leaving L group of PtY_2L_2 dissociating into $(PtY_2L\cdots L)$. [L]Ref. 5. [g]Madelung Potential in Ref. 18. [h]NBO values for Pt and Mulliken values for Ligands in Ref. 3. [i]Ref. 4.

absolute charge values of Pt(II) and Cl in $[PtCl_4]^{2-}$ are smaller than any of the other corresponding values for Pt and L, while the absolute charge values of Pt(II) in $[Pt(OH_2)_4]^{2+}$ and (OH^-) in $[Pt(OH)_4]^{2-}$ are larger than any of the other

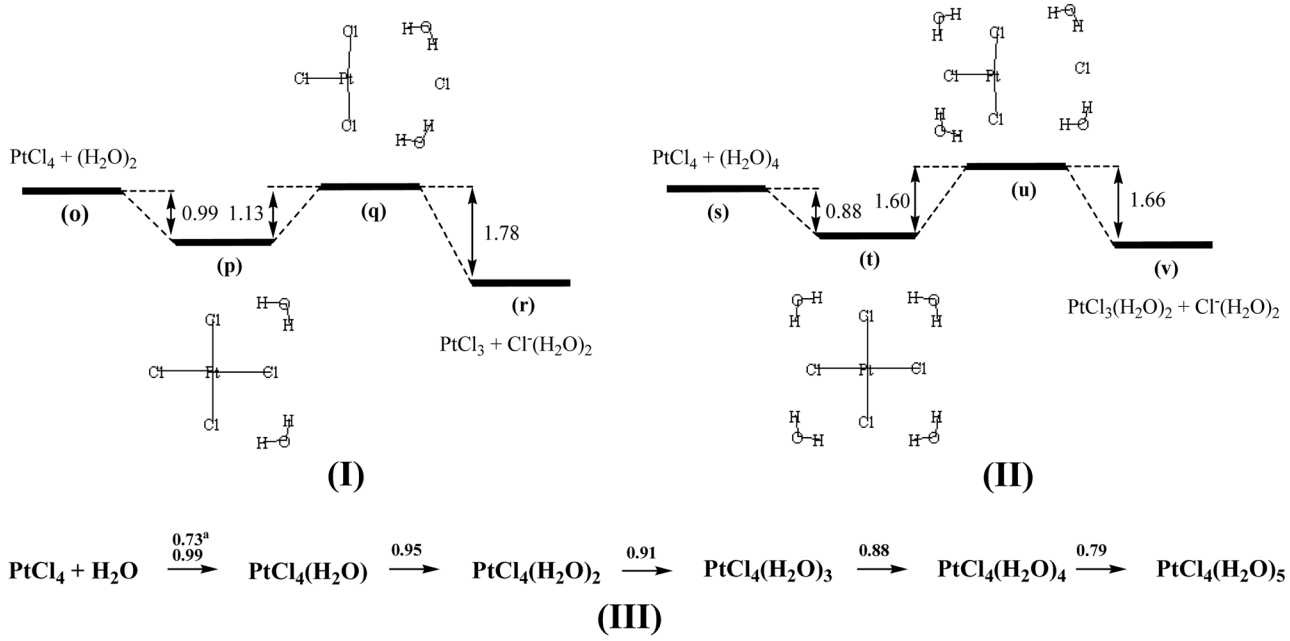

Figure 7. Schematic diagrams for the dissociation energies {**(I)**, **(II)**} of $\{PtCl_4(H_2O)_n(n = 2,4)\}$ into $\{PtCl_3(H_2O)_{(n-2)} + Cl^-(H_2O)_2\}$ and the binding energies {**(III)**} of $PtCl_4$ with water molecules at the B1LYP/LANL2DZ level. Unit of relative energies is eV. [a]Binding energy of cisplatin with H_2O cited from Ref. 8.

corresponding values for Pt and L. Using density functional theory (DFT), the atomic charges of the equilibrium geometrical structure of $[PtL_4]^{2-}$ were investigated by Liao and Zhang,[17] Burda *et al*.,[3-5] and Zhang *et al*.[6] In the study of Burda *et al*., the values of Q_{Pt} and Q_L for PtY_2L_2 at the MP2 level are different from those reported in other studies using DFT including our own.

As the (Pt-L) bond distance of $([PtY_2L]^- \cdots L^-)$ increases, the charge variations of Pt(II) and the *trans* L group decrease, while the charge variations of the leaving L^- group increase. Meanwhile, the charges of the *trans* L ligand and leaving L group become increasingly positive and negative, respectively. The charge variation of the *cis* L ligand is constant. In $([Pt(OH)_3]^- \cdots OH^-)$, the average charge variations of the *trans* OH and the leaving OH^- groups are the largest. The atomic charges of the *trans* OH ligand move to the leaving OH^- group *via* the central Pt atom. The charge variations of the leaving OH^- groups are more negative than those of the other leaving L^- groups, that is, charge transfer occurs from the *trans* OH ligand to the leaving OH^- groups. In the asymptote of $([PtY_2L]^- + L^-)$, the leaving L^- groups dissociate to become negative anions. The atomic charge of the leaving groups varies from L^0 to L^-. To reduce the positive charge value of Pt(II) in $([PtY_2L] \cdots L)$, the atomic charge moves from the *trans* and *cis* L ligands to Pt(II). For the dissociation of the (Pt-L) bond, the variations in the atomic charges of Pt(II) and the *trans* L ligand are in line with the variations in the distance of the *trans* L ligand and leaving L^- group.

Schematic diagrams for the dissociation reactions of $\{PtCl_4(H_2O)_n(n = 2,4)\}$ into $\{PtCl_3(H_2O)_{(n-2)} + Cl^-(H_2O)_2\}$ and the binding energies of $PtCl_4$ with water molecules are represented in Figure 7. The geometrical structures of $\{PtCl_4(H_2O)_n(n = 2,4)\}$ are nearly planar. At (p) of (**I**), the binding energy is 0.99 eV. $R_{Pt\text{-}Cl}$ and $R_{Cl\cdots H}$ are about 2.50 and 2.39 Å, respectively. At the (q) state, the potential energy barrier is 1.13 eV. $R_{Pt\cdots Cl}$ and $R_{Cl\cdots H}$ are about 5.01 and 2.22 Å, respectively. The relative energy between the reactant and product asymptotes is 1.64 eV. At (t) of (**II**), the binding energy is 0.88 eV. $R_{Pt\text{-}Cl}$ and $R_{Cl\cdots H}$ are about 2.47 and 2.42 Å, respectively. At the (u) state, the potential energy barrier is 1.60 eV. $R_{Pt\cdots Cl}$ and $R_{Cl\cdots H}$ are about 5.20 and 2.31 Å, respectively. The relative energy between the reactant and product asymptotes is 0.94 eV. For the dissociation reaction of $\{PtCl_4(H_2O)_n(n = 2,4)\}$ into $\{PtCl_3(H_2O)_{(n-2)} + Cl^-(H_2O)_2\}$, the potential barrier of $\{PtCl_4(H_2O)_4\}$ is higher than that of $\{PtCl_4(H_2O)_2\}$ by 0.5 eV. The reaction involving the formation of $\{PtCl_3(H_2O)_{(n-2)}(n = 2,4) + Cl^-(H_2O)_2\}$ from $\{PtCl_4 + (H_2O)_n\}$ is exothermic. As shown in **(III)** of the Figure, the binding energies of $PtCl_4$ with water molecules are calculated for the first time here. Thus, our binding energies can not be compared with previous calculated values. With increasing water molecule size, the interaction becomes weaker. The binding energies decrease stepwise. In pentamer complex of $\{PtCl_4(H_2O)_5\}$, since the cationic character of the Pt(II) core cation is transmitted to the terminal hydrogen, the growth of the water at the second shell is easily combined without the loss of cationic character. That is, although the fifth water is located at the second shell, the binding energy decreases at a regular rate.

Conclusion

We investigated the geometrical structures and potential

energy surfaces for the ligand exchange reactions of tetra-coordinated platinum (PtY_2L_2) complexes in relation to their ligand-solvent interactions. The geometrical structures of the Pt complexes are optimized to the distorted square planar types. The potential energy surfaces for the ligand exchange processes involving the reactant {($[Pt(NH_3)_2Cl_2]\cdots H_2O$), **A**}, the transition state {($[Pt(NH_3)_2Cl]^+\cdots[H_2O][Cl^-]$)‡, **B**}, and the product {($[Pt(NH_3)_2Cl(H_2O)]^+\cdots Cl^-$), **C**} proceeded *via* both hydrogen-bonded and direct metal-solvent interactions. Each reaction surface has one transition state ($[PtY_2L_2\cdots L']^{\ddagger}$) corresponding to complexes such as (Pt-Cl $\cdots$HOH $\cdots$Cl) and (Pt-OH $\cdots$Cl $\cdots$HN). That is, the central Pt(II) metal in ($[PtCl_4\cdots H_2O]^{\ddagger}$ and $[Pt(NH_3)_2Cl_2\cdots H_2O]^{\ddagger}$) interacts with a leaving Cl^- and an entering H_2O, and the entering H_2O simultaneously interacts with a leaving Cl^-. For the reactions involving the conversion of $[Pt(NH_3)_2Cl_2 + H_2O]$ to $[Pt(NH_3)_2Cl(H_2O) + Cl^-]$, the relative energies of **B** with respect to **A** and **C** are 0.79 and 0.34 eV, respectively. For the conversion of ($PtCl_4 + H_2O$) to ($PtCl_3(H_2O) + Cl^-$), the relative energies of **B** with respect to **A** and **C** are 0.91 and 0.08 eV, respectively. The shapes and sizes of the HOMO and LUMO for the exchange reactions vary stepwise with the changes of the reaction coordinates. Due to the charge transfer from the negatively charged OH^- ligand to the positively charged Pt(II) metal, the dissociation energy of (Pt-OH) is the largest. *In the replacement of one or more Cl^- ions with water or ammonia molecules, the possible reaction mechanisms of the ligand exchange in the square-planar complexes simultaneously imply ligand-solvent ($PtY_2L_2\cdots L'$) and metal-solvent ($Y_2L_2Pt\cdots L'$) interactions.* For the dissociation reaction of {$PtCl_4(H_2O)_n(n = 2,4)$} into {$PtCl_3(H_2O)_{(n-2)} + Cl^-(H_2O)_2$}, the potential barrier of {$PtCl_4(H_2O)_4$, **(I)**} is higher than that of {$PtCl_4(H_2O)_2$, **(II)**} by 0.5 eV. The reaction involving the formation of {$PtCl_3(H_2O)_{(n-2)}(n = 2,4) + Cl^-(H_2O)_2$} from {$PtCl_4 + (H_2O)_n$} is exothermic. With increasing water molecule size, the interaction becomes weaker. The binding energies decrease stepwise.

Acknowledgment. This research was supported by a grant (code : F0004021) from the Information Display R&D Center, one of the 21st Century Frontier R&D Programs funded by the Ministry of Commerce, Industry and Energy of the Korean Government.

References

1. Deeth, R. J.; Elding, L. I. *Inorg. Chem.* **1996**, *35*, 5019.
2. Deeth, R. J. *Chem. Phys. Lett.* **1996**, *261*, 45.
3. Burda, J. V.; Zeizinger, M.; Šponer, J.; Leszczynski, J. *J. Chem. Phys.* **2000**, *113*, 2224.
4. Zeizinger, M.; Burda, J. V.; Šponer, J.; Kapsa, V.; Leszczynski, J. *J. Phys. Chem. A* **2001**, *105*, 8086.
5. Burda, J. V.; Zeizinger, M.; Leszczynski, J. *J. Chem. Phys.* **2004**, *120*, 1253.
6. Zhang, Y.; Guo, Z.; You, X.-Z. *J. Am. Chem. Soc.* **2001**, *123*, 9378.
7. Cost, L. A. S.; Rocha, W. R.; De Almeida, W. B.; Dos Santos, H. F. *J. Chem. Phys.* **2003**, *118*, 10584.
8. Chval, Z.; Sip, M. *J. Mol. Struct.* **2000**, *532*, 59.
9. Ayala, R.; Marcos, E. S.; Daz-Moreno, S.; Solë, V. A.; Muòoz-Pãez, A. *J. Phys. Chem. B* **2001**, *105*, 7588.
10. Naidoo, K. J.; Klatt, G.; Koch, K. R.; Robinson, D. J. *Inorg. Chem.* **2002**, *41*, 1845.
11. Wysokinski, R.; Michalska, D. *J. Comput. Chem.* **2001**, *22*, 901.
12. Hush, N. S.; Schamberger, J.; Bacskay, G. B. *Coor. Chem. Rev.* **2005**, *249*, 299.
13. Park, J. K.; Kim, B. G.; Koo, I. S. *Bull. Korean Chem. Soc.* **2005**, *26*, 1795.
14. Park, J. K.; Cho, Y. G.; Lee, S. S.; Kim, B. G. *Bull. Korean Chem. Soc.* **2004**, *25*, 85.
15. Caminiti, R.; Carbone, M.; Sadun, C. *J. Mol. Liquid* **1998**, *75*, 149.
16. Hay, P. J. *J. Am. Chem. Soc.* **1981**, *103*, 1390.
17. Noell, J. O.; Hay, P. J. *Inorg. Chem.* **1982**, *21*, 14.
18. Liao, M.-s.; Zhang, Q.-er. A *Inorg. Chem.* **1997**, *36*, 396.
19. Ponec, R.; Øeøicha, R. *J. Organomet. Chem.* **1988**, *431*, 549.
20. Carloni, P.; Andreoni, W.; Hutter, J.; Curioni, A.; Giannozzi, P.; Parrinello, M. *Chem. Phys. Lett.* **1995**, *234*, 50.
21. Pavankumar, P. N.; Seetharamulu, P.; Yao, S.; Saxe, J. D.; Reddy, D. G.; Hausheer, F. H. *J. Comput. Chem.* **1999**, *20*, 365.
22. Atoji, M.; Richardson, J. W.; Rundle, R. E. *J. Am. Chem. Soc.* **1957**, *79*, 3017.
23. Milburn, G. H. W.; Truter, M. R. *J. Chem. Soc. A* **1966**, 1609.
24. Shandles, R.; Schlemper, E. O.; Murmann, R. K. *Inorg. Chem.* **1971**, *10*, 2785.
25. Mais, R. H. B.; Owston, P. G.; Wood, A. M. *Acta Cryst.* **1972**, *B28*, 393.
26. Ohba, S.; Sato, S.; Saito, Y. *Acta Crystallogr.* **1983**, *B39*, 49.
27. Templeton, D. H.; Templeton, L. K. *Acta Crystallogr.* **1985**, *A41*, 365.
28. Bengtsson, L. A.; Oskarsson, A. *Acta Chem. Scand.* **1992**, *46*, 707.
29. Chen, Y.; Christensen, D. H.; Nielsen, O. F.; Hyldtoft, J.; Jacobsen, C. J. H. *Spectrochim. Acta* **1995**, *A51*, 595.
30. Frish, M. J.; Trucks, G. W.; Head-Gordon, M. H.; Gill, P. M. W.; Wong, M. W.; Foresman, J. B.; Johnson, B. G.; Schlegel, H. B.; Robb, M. A.; Replogle, E. S.; Gomperts, R.; Andres, J. L.; Raghavachari, K.; Binkley, J. S.; Gonzalez, C.; Martin, R. L.; Fox, D. J.; Defrees, D. J.; Baker, J.; Stewart, J. J. P.; Pople, J. A. *Gaussian 03*; Gaussian Inc.: Pittsburgh, 2003.
31. (a) Andzelm, J.; Wimmer, E. *J. Chem. Phys.* **1992**, *96*, 1280. (b) Andzelm, J.; Wimmer, E.; Salahub, D. R. *The Challenge of d- and f-Electrons: Theory and Computation*, ACS Symposium Series; Salahub, D. R.; Zerner, M. C., Eds; ACS: Washington D. C., 1989; No. 394, p 228. (c) Andzelm, J. *Density Functional Methods in Chemistry*; Labanowski, J.; Andzelm, J., Eds; Springer-Verlag: New York, 1991; p 155.
32. (a) Becke, A. D. *The Challenge of d- and f-Electrons: Theory and Computation*, ACS Symposium Series, Salahub, D. R.; Zerner, M. C., Eds.; American Chemical Society: Washington D.C., 1989; No. 394; p 166. (b) Becke, A. D. *Phys. Rev.* **1988**, *A38*, 3098. (c) Perdew, J. P. *Phys. Rev.* **1986**, *B33*, 8822.
33. Lee, C.; Yang, W.; Parr, R. G. *Phys. Rev.* **1988**, *B37*, 785.